

Persistification of Robotic Tasks

Gennaro Notomista and Magnus Egerstedt

Abstract—In this paper we propose a control framework that enables robots to execute tasks persistently, i.e., over time horizons much longer than robots’ battery life, which is achieved by ensuring that the energy stored in the batteries of the robots is never depleted. This is framed as a set invariance constraint in an optimization problem whose objective is that of minimizing the distance between the robots’ control inputs and nominal control inputs corresponding to the task that is to be executed. We refer to this process as the *persistification* of a robotic task. Forward invariance of subsets of the state space of the robots is turned into a control input constraint by using control barrier functions. The solution of the formulated optimization problem with energy constraints ensures that the resulting task is persistent. To illustrate the operation of the proposed framework, we consider two tasks whose persistent execution is particularly relevant: environment exploration and environment surveillance. We show the persistification of these two tasks both in simulation and on a team of wheeled mobile robots on the Robotarium.

I. INTRODUCTION

ROBOTIC tasks such as environmental monitoring and exploration, and sensor coverage typically evolve over time horizons that last much longer than the battery life of the robots that are employed to execute them. In this sense, we can say that these tasks are not *persistent* insofar as either the robots cannot complete them before their batteries deplete, or they are required to be executed repeatedly and continuously. If, in the former case, robots can be designed with a longer battery life, in general there are no energy sources that can be employed to realize repeated and continuous task executions.

The objective of this paper is presenting a control framework that provably guarantees the *persistent* execution of robotic tasks. This is achieved by minimally modifying the nominal control inputs corresponding to the task that the robots have to execute in order to ensure the continuous execution of the task. As a result, the robots are allowed to freely execute their task whenever they have enough energy stored in their batteries, whereas they are forced to go and recharge their batteries whenever they are running out of energy.

The deployment of robots for tasks such as environmental monitoring [1], [2], [3], [4], environment exploration [5], [6], [7] and sensor coverage [8], [9], [10] has been extensively investigated. However, despite the fact that, in most cases, these tasks have to be executed over long time horizons, the limited availability of energy is not directly taken into account. Nevertheless, since in many mobile robotic applications,

low energy density is still a severe limiting factor, energy-awareness is a necessary features with which robots have to be endowed [11]. This line of inquiry has been followed in [12], which considers a multi-robot, persistent coverage problem as a variant of the vehicle routing problem. A heuristic algorithm is proposed that is based on the cost-to-go-to-target, which can be adjusted online to take into account detours that pass through refueling stations present in the environment. A different approach is adopted in [13], where a formulation based on Markov decision processes is presented, that is able to ensure persistence surveillance coverage, including communication constraints and sensor failure models.

Energy-aware control policies for persistent surveillance using a team of robots are considered in [14], where an optimization problem is defined in order to trade-off between the coverage mission and the conservation of a desired energy level. This is achieved by transitioning between coverage-directed and charging-directed behaviors, based on the current energy levels. The coverage performances are improved by employing “standby” robots that can be deployed when a robot is docked at a charging station. Similarly, in [15] a solution to the problem of long-duration missions is proposed, which considers the team of robots split into “task robots”, which are in charge of executing tasks, and “delivery robots”, which are deployed with the goal of providing the task robots with the energy resources they request. Also in [16], the strategy consists in making use of a team of robots dedicated to charging tasks (ground mobile docking stations), whose trajectories are planned based on the working robots’ trajectories (UAVs), in order to guarantee rendez-vous and recharge without suspending the operation of the working robots. Limited energy reserve is used as an additional constraint in [17] for a path planning strategy for the optimal deployment of multi-robot teams.

The *persistification* approach, through which a robotic task is rendered persistent, that we present in this paper, leverages control barrier functions (CBFs) to formulate an optimization problem where the task execution is constrained by the robots’ energy level. CBFs are used to synthesize a controller that ensures the forward invariance of a set \mathcal{C} of the robot state space. This way, defining \mathcal{C} as the set where the battery energy level of the robots executing the task is always greater than a desired minimum value, the persistification of a task can be formally guaranteed by ensuring the forward invariance of \mathcal{C} . CBFs have been formally defined for control applications in [18]. In [19], [20], [21], variations have been introduced in order to employ CBFs with different categories of nonlinear dynamic systems for different control applications.

The persistification framework described in the following extends the work in [22]. More specifically, the main contribution of this paper is the reformulation of the task

This work was sponsored by the U.S. Office of Naval Research through Grant No. N00014-15-2115.

G. Notomista (*corresponding author*) is with the School of Mechanical Engineering, Institute for Robotics and Intelligent Machines, Georgia Institute of Technology, Atlanta, GA 30332 USA (email: g.notomista@gatech.edu)

M. Egerstedt is with the School of Electrical and Computer Engineering, Institute for Robotics and Intelligent Machines, Georgia Institute of Technology, Atlanta, GA 30332 USA (email: magnus@gatech.edu)

persistification introduced in [22] in order to be able to handle more complicated robot and energy dynamics. The presented method generalizes to different charging models as well as different robotic tasks. The tasks will be encoded through different nominal inputs to the robots. This allows us to formally guarantee the persistent execution of a large number and variety of robotic tasks.

The remainder of the paper is organized as follows: in Section II, the environment and robot and models considered in this paper are presented and the problem of persistification of robotic tasks is formulated. In Section III, the control framework required to ensure robotic task persistency is introduced and its application is demonstrated by means of preliminary examples. Section IV discusses the application of the presented framework to the persistification of robotic tasks. Section V is dedicated to the validation of the proposed theoretical formulation through the implementation of two robotic tasks, whose persistent execution is particularly relevant, both in simulation and on a team of mobile robots.

II. PROBLEM FORMULATION

The goal of this paper is the persistification of robotic tasks, i. e., ensuring that the battery energy level of the robots executing the tasks never falls below a minimum value. In this section, we introduce the models used for the robots, the environment in which the robots execute their task and the robots' energy dynamics. We conclude the section by formalizing the persistification of robotic tasks.

A. Robot Model

Consider a collection of N robots which are to be deployed to execute a task. The state of robot i , $i = 1, \dots, N$, is denoted by $x_i \in X \subseteq \mathbb{R}^n$. We model the robots using the control affine dynamical system:

$$\dot{x}_i = f(x_i) + g(x_i)u_i, \quad (1)$$

where $u_i \in U \subseteq \mathbb{R}^m$ is robot i 's input, and f and g are two Lipschitz vector fields. Control affine systems arise in many robotic systems, whose dynamics are derived using Euler-Lagrange equations [23], therefore they lend themselves to the description of a large variety of robotic platforms. Throughout this paper, we will assume that the robots are homogeneous, i. e., f and g in (5) are the same for each robot. This assumption does not compromise the proposed persistification strategy, which can be easily extended to the heterogeneous case, as will be explained in Section IV.

The robots considered in this paper are equipped with a rechargeable source of energy, e. g., a battery, and a technology required to recharge it, e. g., solar panels. In the following two subsections, we present a model for the robot energy dynamics which is coupled with the model of the environment in which the robots move. This encompasses, for instance, solar power harvester circuits which employ solar panels to recharge the battery of the robots.

B. Environment Model

The environment, i. e., the domain in which the robots are deployed to perform their task, is represented by the compact set $\mathcal{E} \subset \mathbb{R}^p$, with $p = 2$ or $p = 3$, for ground or aerial robots, respectively. The function

$$\pi : X \subseteq \mathbb{R}^n \mapsto \mathcal{E} \subset \mathbb{R}^p$$

maps the robot state to its position expressed in a Cartesian reference system defined in the environment \mathcal{E} .

Moreover, we consider the time-varying scalar field

$$I : \mathcal{E} \times \mathbb{R}_+ \mapsto \mathcal{I} \subset \mathbb{R}_+, \quad (2)$$

where \mathcal{I} is an interval, defined over the environment, which represents a bounded time-varying non-negative physical quantity (e. g., solar light intensity) associated to each position in \mathcal{E} at each time instant. We insist on I being Lipschitz continuous in its first argument and of class C^1 in its second argument. The need for these assumptions will be explained in the next section.

C. Energy Model

Let $E_i \in \mathbb{R}_+$ be the battery energy level of robot i . The charging and discharging dynamics of the battery are modeled by:

$$\dot{E}_i = F(x_i, E_i, t) = k(w(x_i, E_i, t) - E_i), \quad (3)$$

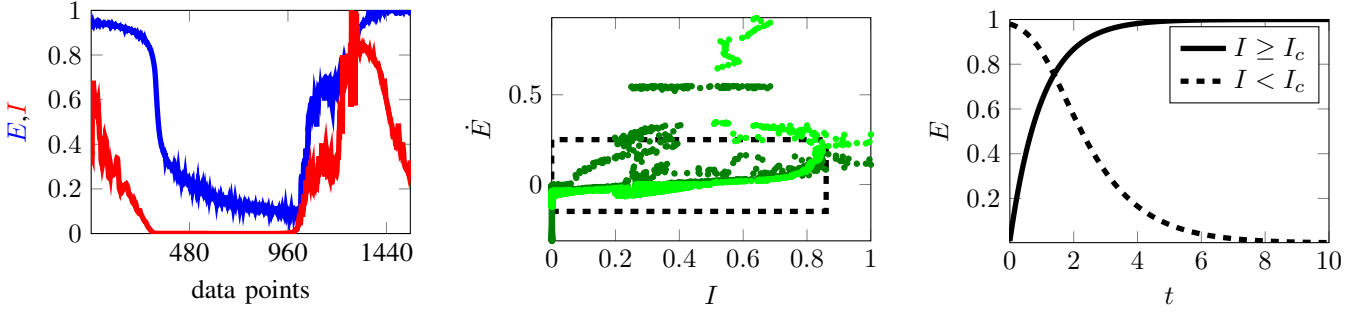
where $k > 0$ and

$$w(x_i, E_i, t) = \frac{1}{1 + \frac{1-E_i}{E_i} e^{-\lambda(I(x_i, t) - I_c)}}. \quad (4)$$

In (4), $\lambda > 0$, $0 < I_c < 1$ and $I(x_i, t) : \mathcal{E} \times \mathbb{R}_+ \mapsto [0, 1]$ is the time-varying scalar-valued function introduced in (2).

The specific expression of $F(x_i, E_i, t)$ has been defined in order to model the exponential charging-discharging dynamics of batteries that are used to power robotic platforms in a large number of applications [24]. In [25], we present the design of a solar-powered robot and report solar intensity and battery charge data collected during the course of a 1-day-long experiment (see Fig. 1a). Fig. 1b shows a comparison between the measurements of Fig. 1a and the predictions of the energy model (3). The measured and the predicted values are depicted in dark and light green, respectively. As can be seen, especially in the region bounded by the dashed rectangle, the model is able to accurately match the energy dynamics. The outliers are mainly due to measurements noise (see Fig. 1a). Moreover, Fig. 1c shows the simulated battery charge and discharge curves obtained using (3): a comparison with Fig. 1a indicates that the theoretical model is able to capture the exponential charging and discharging dynamics of real batteries commonly used for robotics applications.

Remark 1. $I(x_i, t)$ can be interpreted as a time-varying power source distributed over the environment \mathcal{E} . For instance, in the case where it represents a measure of the solar light intensity at the position x_i and time t , $F(x_i, E_i, t)$ can be used to describe the energy dynamics of a solar rechargeable battery. With the given dynamics we have that:



(a) Data collected during the course of a 24-hour experiment using a solar-powered robot. E , in blue, and I , in red, are measured battery energy and solar light intensity, respectively.

(b) Comparison between measured and predicted \dot{E} based on solar light intensity I and battery energy E (shown in Fig. 1a). In the region bounded by the dashed (black) rectangle, the energy model in (3) (light green) is able to accurately match the actual energy dynamics (dark green).

(c) Simulated battery charging and discharging dynamics: a comparison with Fig. 1a shows that the model proposed in (3) is able to reproduce the true dynamics of a real battery used in robotics applications.

Fig. 1. Comparison between the energy model proposed in (3) and data collected during a long-term experiments using a solar-powered robot [25].

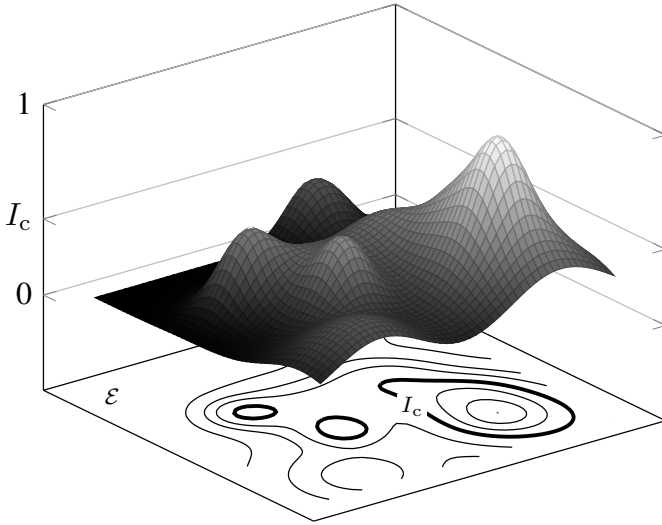
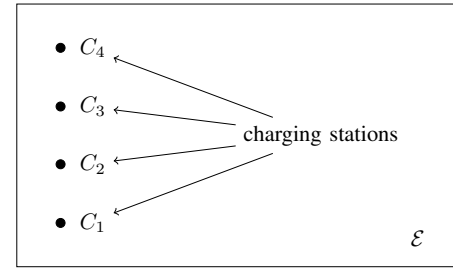


Fig. 2. Example of the function $I(x_i, t)$ over the environment \mathcal{E} at a given time instant: inside the bold level curve marked with I_c , $\dot{E}_i > 0$, whereas outside $\dot{E}_i < 0$. In other words, the robots can recharge their batteries in the regions bounded by the bold curves.

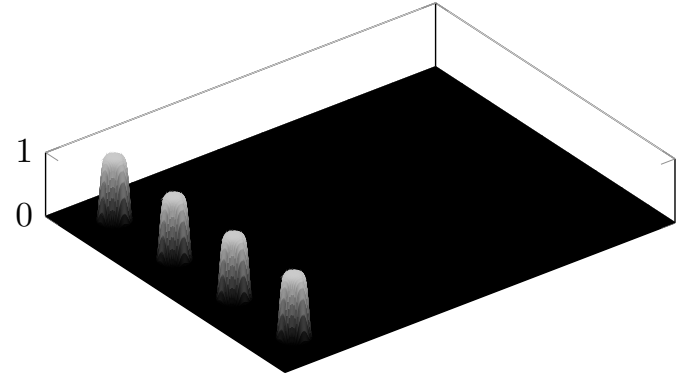
- $\dot{E}_i < 0$, i. e., the battery is discharging, whenever $I(x_i, t) < I_c$
- $\dot{E}_i > 0$, i. e., the battery is charging, when $I(x_i, t) > I_c$
- $\dot{E}_i = 0$, i. e., the value of $I(x_i, t) = I_c$ is such that the generated energy is equal to the energy required by the robot at time t .

Fig. 2 shows an example of what has been described: the surface plot of the function I at a given time instant t is depicted in grayscale (black to white for values of I that go from 0 to 1). Below the surface plot, the contour plot of I highlights the level curves where $I(x_i, t) = I_c$. Inside the regions bounded by the bold curves, characterized by $I(x_i, t) > I_c$, $\dot{E}_i > 0$, i. e., the robots can charge their batteries.

Remark 2. Lumped sources of energy, such as charging stations, can be also modeled using (2). Bump functions [26]



(a)



(b)

Fig. 3. Example of the modeling of lumped sources of energy (charging stations) via a suitable $I(x_i, t)$ function. In Fig. 3a, a rectangular environment \mathcal{E} is shown, and the positions of four charging stations, denoted by C_1 to C_4 , are depicted as black dots. Fig. 3b shows the surf plot of $I(x_i, t)$ corresponding to the charging stations of Fig. 3a modeled by means of bump functions.

at the locations of the charging stations supported in subsets of \mathcal{E} can be employed to obtain the desired charging behavior, as depicted in Fig. 3.

Remark 3. The proposed energy model does not depend on the control input u_i of the robot. At first, this can seem inaccurate, however in Section IV we will show why this choice was made and how it increases robustness of the proposed persistification approach, ensuring that the robots will never run out of energy while executing the given task.

D. Task Persistification

The compound model of robot and energy dynamics is given by the following set of differential equations:

$$\begin{cases} \dot{x}_i = f(x_i) + g(x_i)u_i \\ \dot{E}_i = F(x_i, E_i, t). \end{cases} \quad (5)$$

Indicating by $z_i = [x_i^T, E_i]^T$ the augmented state of robot i , (5) can be rewritten in the following control affine form:

$$\dot{z}_i = \hat{f}(z_i, t) + \hat{g}(z_i)u_i, \quad (6)$$

where

$$\hat{f}(z_i, t) = \begin{bmatrix} f(x_i) \\ F(x_i, E_i, t) \end{bmatrix} \quad \text{and} \quad \hat{g}(z_i) = \begin{bmatrix} g(x_i) \\ 0 \end{bmatrix}.$$

We will use

$$x = \begin{bmatrix} x_1 \\ \vdots \\ x_N \end{bmatrix} \in X^{Nn}, \quad u = \begin{bmatrix} u_1 \\ \vdots \\ u_N \end{bmatrix} \in U^{Nm}$$

to represent the joint states and inputs of the N robots performing the task to be persistified.

Let the task that has to be executed by the robots be encoded through the nominal input

$$\hat{u}_i(x, t), \quad i = 1, \dots, N,$$

or collectively as:

$$\hat{u} : X^{Nn} \times \mathbb{R}_+ \mapsto U^{Nm}. \quad (7)$$

Examples of \hat{u} for the execution of particular robotic tasks will be given in Section IV.

Definition 4 (Task Persistification). *A task encoded through the nominal input \hat{u} , defined in (7), is persistified if the robots employed to perform it execute the input u^* , solution of the following program:*

$$\begin{aligned} u^*(x, t) = \underset{u}{\operatorname{argmin}} \|u - \hat{u}(x, t)\|^2 \\ \text{s.t. } E_i(t) \in [E_{\min}, E_{\text{chg}}] \end{aligned} \quad (8)$$

$\forall t \geq 0, \forall i \in \{1, \dots, N\}$, where E_i is the energy of robot i introduced in Section II-C, and $E_{\min} > 0$ and E_{chg} , with $1 \geq E_{\text{chg}} > E_{\min} > 0$, are the minimum and the maximum energy values, respectively, between which the energy of the robots should be confined.

Task persistification is referred to as the process of turning a task characterized by the nominal input \hat{u} to the persistified task characterized by the input u^* .

Remark 5. *Definition 4 is not tailored to the specific robot and environment models, which, as a matter of fact, can be quite different from the ones presented above, depending on the particular application that is being considered. Nevertheless, the defined task persistification process remains the same.*

III. CONTROL FRAMEWORK

As explained in Section I, the task persistification expressed as the optimization problem (8), will be realized by employing control barrier functions (CBFs). In the following subsection, we give a brief introduction to CBFs in their basic form. Then, in Section III-B, we present the extensions that represent the main theoretical contribution of this paper, namely a flexible framework to deal with time-varying and high relative degree CBFs and CLFs. The results obtained in this section will be used to deal with high relative degree control Lyapunov functions as well, and will be employed in Section IV to formulate the quadratic program whose solution realizes the persistification of robotic tasks.

A. Control Barrier Functions

Introduced in [18], control barrier functions have been used with the goal of ensuring *safety*, intended as the invariance property of a subset of the state space, the *safe set*. In the following we give the extended definition introduced in [27] which will be used throughout this paper.

Definition 6 ([27]). *Let $h : X \subset \mathbb{R}^n \rightarrow \mathbb{R}$ be a continuously differentiable function, and \mathcal{C} its zero superlevel set, i. e., $\mathcal{C} = \{x \in \mathbb{R}^n \mid h(x) \geq 0\}$. Then, for a control affine system*

$$\dot{x} = f(x) + g(x)u, \quad (9)$$

$x \in X \subset \mathbb{R}^n, u \in U \subset \mathbb{R}^m, h$ is a control barrier function (CBF) if there exists a locally Lipschitz extended class \mathcal{K} function [27] α such that

$$\sup_{u \in U} [L_f h(x) + L_g h(x)u + \alpha(h(x))] \geq 0,$$

for all x in the interior of the set \mathcal{C} . $L_f h(x)$ and $L_g h(x)$ represent the Lie derivative of h in the directions of the vector fields f and g , respectively.

Starting from this basic definition, in the next sections we will develop tools required for the persistification of robotic tasks.

B. High Relative Degree CBFs and CLFs

In the previous section, we introduced the robot and energy models. In Remark 3, we have pointed out that the energy dynamics do not depend explicitly on the robot input u_i . This is intended to be a conservative choice which increase the robustness of the persistification strategy. In fact, the rate of charge and discharge of the battery, obtained when $I(x_i, t) = 1$ and $I(x_i, t) = 0$, respectively, are designed to be the slowest recharge rate and the fastest discharge rate obtained when the robot input u_i attains its maximum value. This would correspond, for instance, to the fastest discharge rate obtained when the actuators of the robot are providing maximum power. Then, the actual discharge rate will always be slower than the modeled one, increasing, this way, the robustness of the proposed persistification strategy against unmodeled phenomena which can occur in the environment, or unmodeled robot dynamics.

Nevertheless, the gained robustness comes at the price of increasing the relative degree of the CBF h , defined below, as will be shown later in Section IV

Definition 7 (Relative degree of a CBF, based on [20]). *Given the nonlinear system (9), with f and g sufficiently smooth vector fields on a domain \mathcal{D} , the CBF $h : \mathbb{R}^n \mapsto \mathbb{R}$ has relative degree ρ , $1 \leq \rho \leq n$, in $\mathcal{D}_0 \subset \mathcal{D}$ if the system*

$$\begin{cases} \dot{x} = f(x) + g(x)u \\ y = h(x) \end{cases}$$

has relative degree ρ , $\forall x \in \mathcal{D}_0$.

In the following, we give an example in which high relative degree CBFs [20] are required. This example will be generalized in Theorem 9 for arbitrary high relative-degree CBFs. Then, Theorem 9 will be applied in order to formulate an optimization program which realizes the proposed persistification strategy.

Example 8 (Cascade of CBFs). *Let us consider the nonlinear dynamical system in control affine form (9) and a sufficiently smooth function $h_1 : \mathbb{R}^n \mapsto \mathbb{R}$ with relative degree 2 (i. e., $L_g h_1(x) = 0$ and $L_g L_f h_1(x) \neq 0$) that defines the superlevel set $\mathcal{C}_1 = \{x \in \mathbb{R}^n \mid h_1(x) \geq 0\}$. To prove the forward invariance of the set \mathcal{C}_1 , we want h_1 to be a CBF that means that the following must hold:*

$$L_f h_1(x) + \alpha_1(h_1(x)) \geq 0,$$

where α_1 is a locally Lipschitz extended class \mathcal{K} function, and we used the fact that h_1 has relative degree 2. Then, we can define an additional function

$$h_2(x) = L_f h_1(x) + \alpha_1(h_1(x)) \quad (10)$$

that defines the set $\mathcal{C}_2 = \{x \in \mathbb{R}^n \mid h_2(x) \geq 0\}$. If there exists a positive constant γ_1 and a locally Lipschitz extended class \mathcal{K} function α_2 such that:

$$\sup_{u \in U} [L_f^2 h_1(x) + L_g L_f h_1(x) u + \gamma_1 L_f h_1(x) + \alpha_2(h_2(x))] \geq 0, \quad (11)$$

the function h_2 is a CBF. The expression of (11) for arbitrary high relative degree will be given in the next theorem. The existence of the CBF $h_2(x)$ ensures the forward invariance of the set \mathcal{C}_2 , which, in turns, ensures the existence of the CBF $h_1(x)$. The forward invariance of the set \mathcal{C}_1 is thus proved.

The technique shown in example 8 is generalized in the following theorem.

Theorem 9. *Given a dynamical system (9), a sufficiently smooth CBF $h_1(x)$ with relative degree ρ and a CBF $h_\rho(x)$ recursively evaluated as*

$$h_{n+1}(x) = \dot{h}_n(x) + \alpha_n(h_n(x)), \quad (12)$$

with α_n locally Lipschitz extended class \mathcal{K} functions, we define the set $K_\rho(x)$ as

$$K_\rho(x) = \left\{ u \in U \mid L_f^\rho h_1(x) + L_g L_f^{\rho-1} h_1(x) u + \sum_{i=1}^{\rho-1} \sum_{\mathcal{C} \in \binom{[\rho-1]}{i}} \prod_{j \in \mathcal{C}} \frac{\partial \alpha_j}{\partial h_j} L_f^{\rho-i} h_1(x) + \alpha_\rho(h_\rho(x)) \geq 0 \right\},$$

where $\binom{[\rho-1]}{i}$ is the set of i -combinations from the set $\{1, \dots, \rho-1\} \subset \mathbb{N}$ and α_j , $j = 1, \dots, \rho$ are extended class \mathcal{K} functions. Then, any Lipschitz continuous controller $u \in K_\rho(x)$ will render the set $\mathcal{C}_1 = \{x \in \mathbb{R}^n \mid h_1(x) \geq 0\}$ forward invariant.

Proof. Given the properties of class \mathcal{K} functions [28] and using the fact that $h_1(x)$ has relative degree ρ , $\dot{h}_\rho(x)$ is given by the following expression:

$$\begin{aligned} \dot{h}_\rho &= L_f^\rho h_1(x) + L_g L_f^{\rho-1} h_1(x) u \\ &+ \sum_{i=1}^{\rho-1} \sum_{\mathcal{C} \in \binom{[\rho-1]}{i}} \prod_{j \in \mathcal{C}} \frac{\partial \alpha_j}{\partial h_j} L_f^{\rho-i} h_1(x). \end{aligned}$$

Consequently, the choice of $u \in K_\rho(x)$ renders the set $\mathcal{C}_\rho = \{x \in \mathbb{R}^n \mid h_\rho(x) \geq 0\}$ forward invariant. By recursively applying (12) $\rho-1$ times, \mathcal{C}_1 is proved to be forward invariant. \square

Remark 10. *Employing a cascade of CBFs as shown in Example 8 and in Theorem 9 is a technique which can be used not only to prove set forward invariance, but also stability of dynamical systems using high relative degree Lyapunov functions, as will be shown later in this section. Set forward invariance and stability will be used, in Section IV, to ensure that the energy stored in the battery of the robots performing a task is never depleted, realizing, this way, the desired task persistification.*

Note that the energy model proposed in Section II-C is time-dependent, as it depends on the environment model, namely on the value $I(x_i, t)$ at x_i at time t . As we are going to use CBFs to ensure the persistent execution of a task, we now extend the notion of CBFs to the case in which the function h that defines the safe set \mathcal{C} , depends explicitly on a time variable.

For the nonlinear control affine system (9), we wish to ensure the forward invariance of a set $\mathcal{C} \subset \mathbb{R}^n$ defined by the superlevel set of a function $h : \mathbb{R}^n \times \mathbb{R}_+ \mapsto \mathbb{R}$ as:

$$\mathcal{C} = \{x \in \mathbb{R}^n \mid h(x, t) \geq 0\}. \quad (13)$$

With this objective, we extend the definition CBFs given in [27] to the time-varying case.

Definition 11 (Time-Varying CBFs). *Given a dynamical system (9) and a set \mathcal{C} defined in (13), the function h is a time-varying CBF defined on $\mathcal{D} \times \mathbb{R}_+$, with $\mathcal{C} \subseteq \mathcal{D} \subset \mathbb{R}^n$, if there exists a locally Lipschitz extended class \mathcal{K} function α such that, $\forall x \in \mathcal{D}$,*

$$\sup_{u \in U} \left[\frac{\partial h}{\partial t} + L_f h(x, t) + L_g h(x, t) u + \alpha(h(x, t)) \right] \geq 0. \quad (14)$$

Starting from the condition in (14), we can define the set:

$$K(x, t) = \left\{ u \in U \left| \begin{aligned} & \frac{\partial h}{\partial t} + L_f h(x, t) + L_g h(x, t) u \\ & + \alpha(h(x, t)) \geq 0 \end{aligned} \right. \right\}. \quad (15)$$

The following lemma ensures that the set \mathcal{C} , defined in (13), is rendered forward invariant by the application of a control input $u \in K(z, t)$. This result will be used in Section IV to express the constraints on the energy in (8) in terms of the control input u .

Lemma 12. *Given a set \mathcal{C} defined as in (13), if h is a time-varying CBF on $\mathcal{D} \times \mathbb{R}_+$, then any Lipschitz continuous controller $u : \mathcal{D} \mapsto U$ such that $u \in K(x, t)$, where $K(x, t)$ is given in (15), will render the set \mathcal{C} forward invariant.*

Proof. (Following the proof of Theorem 1 in [18]) If h is a time-varying CBF on $\mathcal{D} \times \mathbb{R}_+$ and $u \in K(x, t)$, from (14) and (15) we can derive the following differential inequality:

$$\dot{h}(x, t) \geq -\alpha(h(x, t)). \quad (16)$$

Now, consider the following boundary condition problem:

$$\begin{cases} \dot{\zeta} = -\alpha(\zeta) \\ \zeta(t_0) = h(x(t_0), t_0) > 0, \end{cases}$$

whose solution is given by $\zeta(t) = \beta(\zeta(t_0), t - t_0)$, β being a class \mathcal{KL} function (Lemma 4.4 in [29]). From (16), making use of the Comparison Lemma (Lemma 3.4 in [29]), we have that:

$$h(x(t), t) \geq \beta(\zeta(t_0), t - t_0), \quad \forall t \geq t_0. \quad (17)$$

Hence, if $h(x(t_0), t_0) > 0$ and therefore $x(t_0) \in \mathcal{C}$, using the properties of class \mathcal{KL} functions, (17) ensures that $h(x(t), t) > 0 \forall t \geq t_0$ and so $x(t) \in \mathcal{C} \forall t \geq t_0$. Thus, \mathcal{C} is forward invariant. \square

Remark 13. *In case $\frac{\partial h}{\partial t} = 0$ and $L_g h(x, t) = 0$ we are not able to ensure the existence of a control input such that (14) holds, condition on which Lemma 12 relies. This case can be tackled by making use of a cascade of control barrier functions and the result of Theorem 9.*

So far, we have described the condition in which the robots are executing the assigned task and we want them to keep their energy level E_i within a certain interval $[E_{\min}, E_{\text{chg}}]$. This is realized, employing CBFs, by letting the robots reach regions of the state space where the field I introduced in (2) is larger than I_c . In this regions, as observed in Remark 1, $\dot{E}_i > 0$ and the robots are charging.

To make sure that the robots leave the *charging stations*, intended in a broader sense as the regions of the state space where $I(x_i, t) \geq I_c$, only when their battery is fully charged, i.e., when $E_i \approx E_{\text{chg}}$, we will employ control Lyapunov functions (CLFs). Similarly to what happens with CBFs encoding energy constraints, since the input u_i does not directly show up in the expression of \dot{E}_i , a CLF defined to fully recharge the robots' battery will have relative degree higher than 1. Therefore, in the following, we are going to proceed

analogously to what has been done for high relative degree CBFs to handle the case of high relative degree CLFs.

Suppose that, besides the forward invariance of a set, one would like to stabilize the dynamical system (9) around the origin $x = 0$ using a CLF. Similarly to what has been done for the CBFs, the existence of a CLF $V : \mathbb{R}^n \mapsto \mathbb{R}$ suggests the definition of the following set:

$$K_V(x) = \{u \in U \mid -L_f V(x) - L_g V(x) u \geq 0\}.$$

The choice of a control input $u \in K_V(x)$ will stabilize the system around $x = 0$.

Remark 14. *In case $L_g V(x) = 0$, i.e., the relative degree of the Lyapunov function is greater than 1, we cannot ensure that the origin is stable.*

In Example 8 and in Theorem 9, a technique for dealing with high relative degree control barrier functions has been introduced: we will proceed here in a similar fashion. We first give an example that shows how to construct high-relative degree CLFs by employing CBFs. Then, we generalize this construction in Theorem 16.

Example 15 (Constructing high relative degree CLFs using CBFs). *Let us consider the nonlinear dynamical system in control affine form (9) and a sufficiently smooth function $V : \mathbb{R}^n \mapsto \mathbb{R}$ with relative degree 2, i.e., $L_g V(x) = 0$ and $L_g L_f V(x) \neq 0$. In order for V to be a CLF we must have $-L_f V(x) > 0$. We can then define the CBF $h_1(x) = -L_f V(x)$, and its superlevel set $\mathcal{C}_1 = \{x \in \mathbb{R}^n \mid -L_f V(x) \geq 0\}$, and let $u \in K'_2(x) = \left\{ u \in U \mid -L_f^2 V(x) - L_g L_f V(x) u + \alpha(-L_f V(x)) \geq 0 \right\}$. This way, under certain conditions that will be made explicit in the following theorem, the set \mathcal{C}_1 is forward invariant and, consequently, the existence of the CLF $V(x)$ guarantees that the origin $x = 0$ is (asymptotically) stable.*

Theorem 16. *Consider the dynamical system (9), a CLF $V(x)$ with relative degree ρ defined with the objective of stabilizing the system to $x = x^*$ and a CBF $h_\rho(x)$ recursively evaluated as follows:*

$$\begin{cases} h_1(x) = -L_f V(x) \\ h_{n+1}(x) = \dot{h}_n(x) + \alpha_n(h_n(x)), \end{cases} \quad (18)$$

where α_n are locally Lipschitz extended class \mathcal{K} functions. In addition, assume that $\{x^*\}$ is the largest invariant set in $\partial\mathcal{C}_1 = \{x \mid h_1(x) = 0\}$, boundary of the set $\mathcal{C}_1 = \{x \mid h_1(x) \geq 0\}$. Then, any Lipschitz continuous controller

$$u \in K'_\rho(x) = \left\{ u \in U \mid \begin{aligned} & -L_f^\rho V(x) - L_g L_f^{\rho-1} V(x) u \\ & + \sum_{i=1}^{\rho-2} \sum_{\mathcal{C} \in (\mathcal{C}_i^{\rho-2})} \prod_{j \in \mathcal{C}} \frac{\partial \alpha_j}{\partial h_j} (-L_f^{\rho-1-i} V(x)) + \alpha_\rho(h_\rho(x)) \geq 0 \end{aligned} \right\},$$

will asymptotically stabilize the system to $x = x^*$.

Proof. Given the properties of class \mathcal{K} functions and using the fact that $h_1(x) = -L_f V(x)$ has relative degree $\rho - 1$, the following expression of h_ρ can be derived:

$$\begin{aligned} \dot{h}_\rho(x) &= -L_f^\rho V(x) - L_g L_f^{\rho-1} V(x) u \\ &+ \sum_{i=1}^{\rho-2} \sum_{\mathcal{C} \in \binom{[\rho-2]}{i}} \prod_{j \in \mathcal{C}} \frac{\partial \alpha_j}{\partial h_j} (-L_f^{\rho-1-i} V(x)). \end{aligned}$$

The choice of $u \in K'_\rho(x)$ will render the set $\mathcal{C}_\rho = \{x \in \mathbb{R}^n \mid h_\rho(x) \geq 0\}$ forward invariant. Similarly to what has been done in Theorem 9, by the recursive application of (18), \mathcal{C}_1 is proven to be forward invariant. Then, by LaSalle's Theorem (Theorem 4.4 in [29]), as $\{x^*\}$ is the largest invariant set in $\partial\mathcal{C}_1$, one has that $x(t) \rightarrow x^*$ as $t \rightarrow \infty$. \square

IV. APPLICATION TO ROBOTIC TASKS

In view of what has been introduced in the previous section, in this section we show that the persistification of robotic tasks, specified in Definition 4, can be framed as an optimization problem.

In order for the robots to be able to perpetually execute the given task, their energy E_i , $i = 1, \dots, N$ must be strictly greater than zero at each point in time. Moreover, in order to extend the battery life of the specific types of batteries used in robotic applications, the lower bound for the residual energy should not be too low in order to protect the battery from deep discharge [30]. Considering the simplified single integrator dynamics robot model in lieu of (5), the constraints to control the residual energy can be formally encoded by the following CBF related to robot i :

$$h_{i1}(z_i) = (E_{\text{chg}} - E_i)(E_i - E_{\min}), \quad (19)$$

where E_{chg} and E_{\min} are the upper and lower bounds between which we want the energy E_i to be confined, corresponding to charged and depleted battery, respectively.

Following the procedure adopted in Example 8, we start by evaluating the time derivative of $h_{i1}(z_i)$:

$$\begin{aligned} \dot{h}_{i1}(z_i) &= \frac{\partial h_{i1}}{\partial t} + L_f h_{i1}(z_i) + L_g h_{i1}(z_i) u_i \\ &= \left[\frac{\partial h_{i1}}{\partial x_i} \quad \frac{\partial h_{i1}}{\partial E_i} \right] f(z_i, t) + \left[\frac{\partial h_{i1}}{\partial x_i} \quad \frac{\partial h_{i1}}{\partial E_i} \right] g(z_i) u_i \\ &= (E_{\text{chg}} + E_{\min} - 2E_i) F(x_i, E_i, t), \end{aligned}$$

which does not depend on u_i as the relative degree of $h_{i1}(z_i)$ is 2. Therefore, we define the CBF $h_{i2}(z_i)$ as done in (10), namely:

$$h_{i2}(z_i) = \dot{h}_{i1}(z_i) + \gamma_{i1} h_{i1}(z_i), \quad (20)$$

in which the locally Lipschitz class \mathcal{K} function has been chosen to be a linear function, with $\gamma_{i1} > 0$.

Using Theorem 9 and Lemma 12, we can define the set of control inputs u_i that will render the set $\mathcal{C}_{i1} = \{z_i \mid h_{i1}(z_i) \geq 0\} = \{E_i \mid E_{\min} \leq E_i \leq E_{\text{chg}}\}$ forward invariant:

$$\begin{aligned} K_{2i}(z_i) &= \left\{ u_i \in U_i \mid \frac{\partial h_{i2}}{\partial t} + L_f^2 h_{i1}(z_i) \right. \\ &\left. + L_g L_f h_{i1}(z_i) u_i + \gamma_{i1} L_f h_{i1}(z_i) + \gamma_{i2} h_{i2}(z_i) \geq 0 \right\}, \end{aligned}$$

in which $\gamma_{i2} h_{i2}(z_i)$, with $\gamma_{i2} > 0$, is the locally Lipschitz extended class \mathcal{K} function $\alpha_2(h_2)$ in (11). The expressions of $\frac{\partial h_{i2}}{\partial t}$, $L_f^2 h_{i1}(z_i)$ and $L_g L_f h_{i1}(z_i)$ are reported in full in Appendix A.

Note that, due to the control affine form of (6), $u_i \in K_{2i}(z_i)$ is an affine constraint in u_i and therefore it can be written as:

$$A_{\text{CBFi}}(z_i) u_i \leq b_{\text{CBFi}}(z_i), \quad (21)$$

with $A_{\text{CBFi}}(z_i) = -L_g L_f h_{i1}(z_i)$ and $b_{\text{CBFi}}(z_i) = \frac{\partial h_{i2}}{\partial t} + L_f^2 h_{i1}(z_i) + \gamma_{i1} L_f h_{i1}(z_i) + \gamma_{i2} h_{i2}(z_i)$.

Remark 17. Recalling the expression of \dot{E} introduced in (3), the behavior resulting by enforcing the constraint (21) is the following: when the battery level E_i is getting close to its minimum value E_{\min} , robot i will drive towards areas of the environment \mathcal{E} where the value of the function $I(x_i, t)$ is such that $\dot{E}_i \geq 0$, i. e., robot i starts recharging its battery.

During operation, the battery of each robot continuously discharges according to the dynamics in (5). The mere application of the constraint (21) prevents the battery level to go lower than E_{\min} or higher than E_{chg} . However, it does not ensure that the battery will be completely charged before robot i leaves areas of the environment where $\dot{E}_i > 0$, as it would be desirable. This behavior can be formulated as a CLF whose objective is that of driving the energy E_i to E_{chg} . We can then define

$$V_i(z_i) = (E_{\text{chg}} - E_i)^2, \quad (22)$$

related to robot i , whose time derivative is given by

$$\begin{aligned} \dot{V}_i(z_i) &= \frac{\partial V_i}{\partial t} + L_f V_i(z_i) + L_g V_i(z_i) u_i \\ &= \left[\frac{\partial V_i}{\partial x_i} \quad \frac{\partial V_i}{\partial E_i} \right] f(z_i, t) + \left[\frac{\partial V_i}{\partial x_i} \quad \frac{\partial V_i}{\partial E_i} \right] g(z_i) u_i \\ &= -2(E_{\text{chg}} - E_i) F(x_i, E_i, t). \end{aligned}$$

As in the case of $h_{i1}(z_i)$ of the previous section, here $V_i(z_i)$ has relative degree 2 and therefore its time derivative is not a function of the control input u_i . Proceeding as before, we define the CBF $h_{i1}(z_i) = -L_f V_i(z_i)$. Its superlevel set $\mathcal{C} = \{z_i \mid h_{i1}(z_i) \geq 0\} = \{z_i \mid \dot{V}_i(z_i) \leq 0\}$ is the set in which the value of the function $V_i(z_i)$ is not increasing. Its boundary $\partial\mathcal{C} = \{z_i \mid h_{i1}(z_i) = 0\}$ is the set where $\dot{V}_i(z_i) = 0$ which, if $\dot{E} \neq 0$, coincides with the surface $\{z_i \mid E_i = E_{\text{chg}}\}$. Therefore, by Theorem 16, if

$$\begin{aligned} u_i \in K'_{2i}(z_i) &= \left\{ u_i \in U_i \mid \frac{\partial h_{i2}}{\partial t} - L_f^2 V_i(z_i) \right. \\ &\left. - L_g L_f V_i(z_i) u_i + \gamma_{i2} h_{i2} \geq 0 \right\}, \end{aligned}$$

with $\gamma_{i2} > 0$, the value of E_i will asymptotically converge to E_{chg} . The expressions of $\frac{\partial h_{i2}}{\partial t}$, $L_f^2 V_i(z_i)$ and $L_g L_f V_i(z_i)$ are also reported in full in Appendix A.

Note that also $u_i \in K'_{2i}(z_i)$ is an affine constraint in u_i , and therefore it can be written as:

$$A_{\text{CLFi}}(z_i) u_i \leq b_{\text{CLFi}}(z_i), \quad (23)$$

with $A_{\text{CLFi}}(z_i) = L_g L_f V_i(z_i)$ and $b_{\text{CLFi}}(z_i) = \frac{\partial h_{i2}}{\partial t} - L_f^2 V_i(z_i) + \gamma_{i2} h_{i2}(z_i)$.

In order to combine the constraints (21) coming from the CBF and (23) coming from the CLF, the following nonlinear program can be formulated:

$$\begin{aligned} u^* = \underset{u, \delta}{\operatorname{argmin}} & \|u - \hat{u}\|^2 + \delta^T \kappa \delta \\ \text{s.t.} & \begin{bmatrix} A_{\text{CBF}}(z_i) & 0_N \\ A_{\text{CLF}}(z_i) & -I_N \end{bmatrix} \begin{bmatrix} u \\ \delta \end{bmatrix} \leq \begin{bmatrix} b_{\text{CBF}}(z_i) \\ b_{\text{CLF}}(z_i) \end{bmatrix}, \end{aligned} \quad (24)$$

where the inequality symbol denotes component-wise inequality, and where

$$\begin{aligned} A_{\text{CBF}}(z_i) &= \operatorname{diag}(A_{\text{CBF1}}(z_i), \dots, A_{\text{CBFN}}(z_i)), \\ A_{\text{CLF}}(z_i) &= \operatorname{diag}(A_{\text{CLF1}}(z_i), \dots, A_{\text{CLFN}}(z_i)), \\ b_{\text{CBF}}(z_i) &= \begin{bmatrix} b_{\text{CBF1}}(z_i) \\ \vdots \\ b_{\text{CBFN}}(z_i) \end{bmatrix}, \quad b_{\text{CLF}}(z_i) = \begin{bmatrix} b_{\text{CLF1}}(z_i) \\ \vdots \\ b_{\text{CLFN}}(z_i) \end{bmatrix}, \end{aligned}$$

$u = [u_1^T, \dots, u_N^T]$, and I_N and 0_N are $N \times N$ identity and zero matrices, respectively. Moreover, $\delta = [\delta_1, \dots, \delta_N]^T \in \mathbb{R}^N$ is a vector of relaxation parameters introduced to make the constraints (23) always feasible. $\kappa = \operatorname{diag}(\kappa_i)$ is a diagonal weighting matrix for δ . Furthermore, the nominal input \hat{u} is what encodes the task introduced in Definition 4. Both (21) and (23) are affine functions of the optimization variables. Moreover, the cost $\|u - \hat{u}\|^2 + \delta^T \kappa \delta$ is a convex quadratic form. Hence, (24) is a quadratic program (QP) and it can be efficiently solved in an online fashion (see, for example, [31]).

Remark 18. *As discussed in Section II, the proposed persistification approach also works when robots are not homogeneous, i. e., when they have different dynamic models. In fact, in this case, once the constraints of the optimization program (24) have been changed accordingly, the solution u^* guarantees the heterogeneous multi-robot system persistently executes the task characterized by the nominal input \hat{u} .*

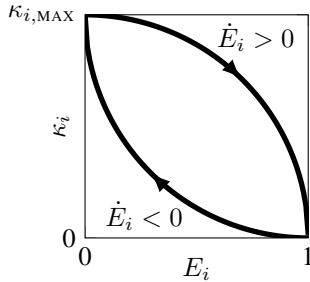


Fig. 4. Example of the function $\kappa_i(E_i)$ that can be employed in order to let robot i charge its battery up to E_{chg} once it has started charging. The two branches of the curve are labeled with $\dot{E}_i > 0$ and $\dot{E}_i < 0$: at a given value of E_i , the value of κ_i is higher for a robot that is recharging its battery ($\dot{E}_i > 0$) compared to the one of a robot for which $\dot{E}_i < 0$. This way, once a robot starts recharging its battery, the weight of its corresponding component of the vector δ in (24) is larger. This ensures that the robot charges its battery until E_{chg} .

Remark 19. *In order to achieve the desired charging behavior, discussed in Section III, κ_i can be made a function of E_i in such a way that robot i charges up to $E_i = E_{\text{chg}}$ once it started charging and, at the same time, discharge down to*

$E_i = E_{\text{min}}$ while operating. A candidate function $\kappa_i(E_i) : [0, 1] \mapsto [0, \kappa_{i, \text{MAX}}]$ is depicted in Fig. 4. Note that the function κ_i changes according to the sign of \dot{E}_i . This way, the weight of the corresponding relaxation parameter δ_i changes when the energy E_i reaches E_{chg} or E_{min} .

The next proposition ensures task persistification as defined in Definition 8.

Proposition 20. *The control law u^* , solution of the QP (24), makes the robots execute the persistified task corresponding to the task encoded through the control input \hat{u} .*

Proof. Immediately follows from the application of Theorem 9, Lemma 12 and Theorem 16. \square

In the next section, the developed theoretical control framework will be validated by means of simulations and experiments. Two robotic tasks are introduced and the results of the their persistent implementation are reported.

V. SIMULATIONS AND EXPERIMENTS

In this section, two robotic tasks, whose persistent application is particularly relevant, are presented as showcases. These are environment exploration and environment surveillance. Both tasks are typically required to be executed for a long period of time. In the case of environment exploration, the long execution time can be due to the size and/or the dynamic nature of the environment [32], [33]. As regards the environment surveillance, the time-scale of the observed environment phenomena determines the length of the task. Nowadays, longevity is still a limiting factor for the deployment of robotic systems for environment surveillance and monitoring [34].

The persistification of these two tasks through the control framework described in the previous section is discussed in Section V-A and Section V-B.

A. Environment Exploration

The first application that is considered is that of environment exploration. There are many approaches to this task in literature, as discussed in Section I, and many solutions have been proposed. Here we consider the one presented in [35], since the result of a trajectory optimization problem provides directly the nominal inputs to the robots. The optimal trajectories are evaluated by minimizing the *distance from ergodicity* using the metric defined in [36]. This results in a trajectory that, instead of maximizing information in a greedy way, distributes information according to its probability density function defined over the environment.

Following what is presented in [35], let us start by defining the following ergodic metric as in [36]:

$$\epsilon = \sum_{k=0}^K \Lambda_k |c_k - \varphi_k|^2, \quad (25)$$

where c_k are the time-averaged Fourier coefficients of the trajectory, φ_k are the Fourier coefficients of a spatial distribution of information $\phi : \mathcal{E} \mapsto \mathbb{R}_+$ and

$$\Lambda_k = \frac{1}{(1 + \xi^T \xi)^{\frac{3}{2}}},$$

with $\xi \in \mathcal{L} = \{0, 1, \dots, K-1\} \times \{0, 1, \dots, K-1\}$, K being the number of employed Fourier basis functions.

By minimizing this ergodic measure at time \bar{t} over a time horizon T , the nominal trajectory $\hat{x}_i(t)$ for $t \in [\bar{t}, \bar{t} + T]$ of each robot is obtained. Solving this optimization problem at every time instant, in a model predictive control fashion, provides the nominal input \hat{u}_i that is to be executed at time \bar{t} in order to track the trajectory \hat{x}_i [35]. This \hat{u}_i can be plugged in the QP defined in (24) allowing, this way, a straightforward application of the persistification framework presented in this paper to the environment exploration task.

The environment exploration task has been implemented and tested in a simulation environment. For the simulated experiment a planar robot is given the task of exploring an environment \mathcal{E} on which a spatial distribution of information has been defined. The information is assumed to be distributed according to the density function

$$\phi : x \in \mathcal{E} \subset \mathbb{R}^2 \mapsto e^{-\frac{\|x-x_0\|^2}{\sigma^2}} \in \mathbb{R}_+,$$

where, for the experiments, the following values are used: $x_0 = [0, 0]^T$ and $\sigma^2 = 0.1$. The time-varying charging field I is modeled as a mixture of time-varying Gaussians of the following form:

$$I(x, t) = e^{-\|x-M_1(t)x_c\|^2} + e^{-\|x-M_2(t)x_c\|^2},$$

where $x_c = [1, 1]^T$ and

$$M_1(t) = \begin{bmatrix} -1 & 0 \\ 0 & \sin(2t) \end{bmatrix}, \quad M_2(t) = \begin{bmatrix} \sin(2t) & 0 \\ 0 & 1 \end{bmatrix}.$$

In the case of robots that are able to exploit solar power to recharge their batteries, this choice of the function I simulates the sunlight intensity that is characterized by a periodic expression over a spatially fixed environment. The other values required to model E_i in (5) are set to: $I_c = 0.85$ and $\lambda = 3$.

The optimization problem aimed at minimizing the ergodic cost (25) is solved offline and the resulting trajectory is given to the robot as a reference for the tracking controller. The input required to track the trajectory is wrapped by the QP (24) in such a way that the robot explores the environment while satisfying at the same time the energy constraint that prevents the battery level to go below the lower threshold E_{\min} . The result of this controller is a persistified environment exploration.

Figures 5a to 5e show a sequence of images taken during the course of the environment exploration experiment described above. The contour plot of the function ϕ is depicted as green thin solid lines, while the contour plot of the charging field I is represented by the yellow thin dashed lines. The position that the robot is tracking under the nominal control input is depicted by a black square, whereas the actual position of the robot executing the controller (24) is represented by a black circle. Furthermore, nominal and executed trajectories are represented by a gray thick solid line and a red thick dashed line, respectively.

Fig. 6 compares the probability density function representing the spatial information distribution ϕ (Fig. 6a) with the

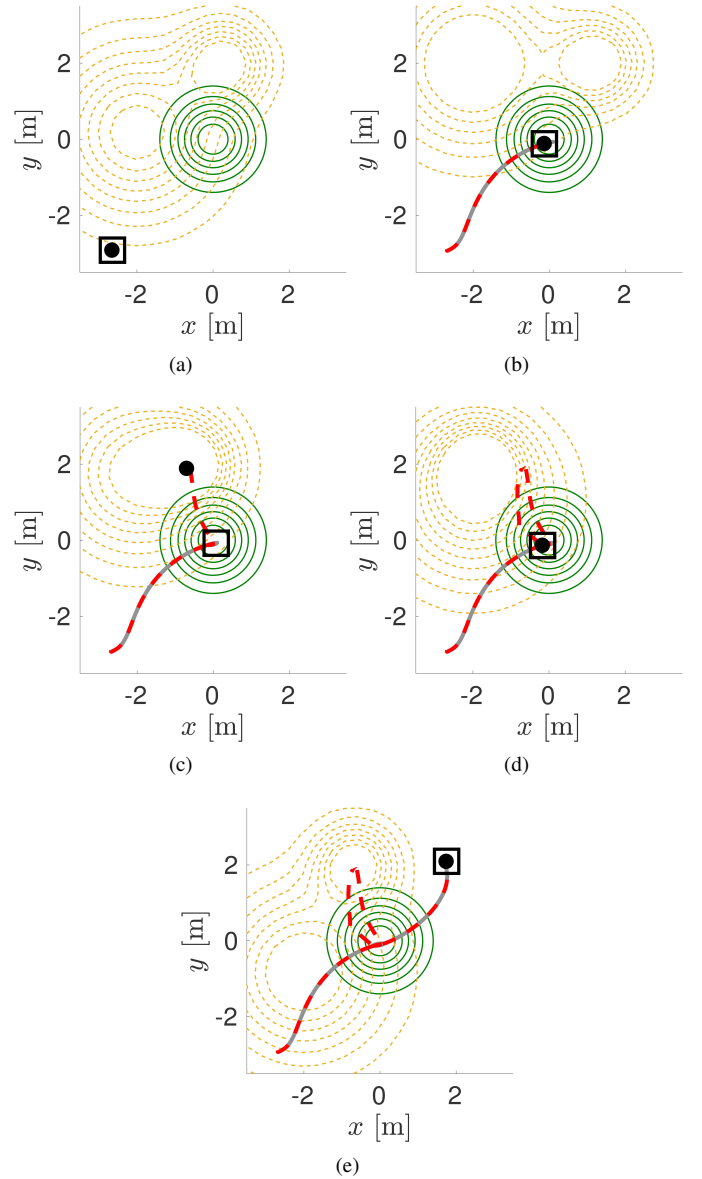


Fig. 5. Sequence of images recorded during the course of the environment exploration simulated experiment. The contour plots of the information distribution function ϕ and the charging field I are depicted as green thin solid and yellow thin dashed lines, respectively. The position tracked by the robot under the nominal control input is represented by a black square, while the actual position of the robot is shown as a black circle. The nominal and actual trajectories are depicted as gray thick solid and a red thick dashed line, respectively. In order to persistently explore the environment, the robot follows the nominal input as long as its energy level is high enough. When its battery is depleting, it moves towards regions of the environment where the value of the field I is such that its energy starts increasing.

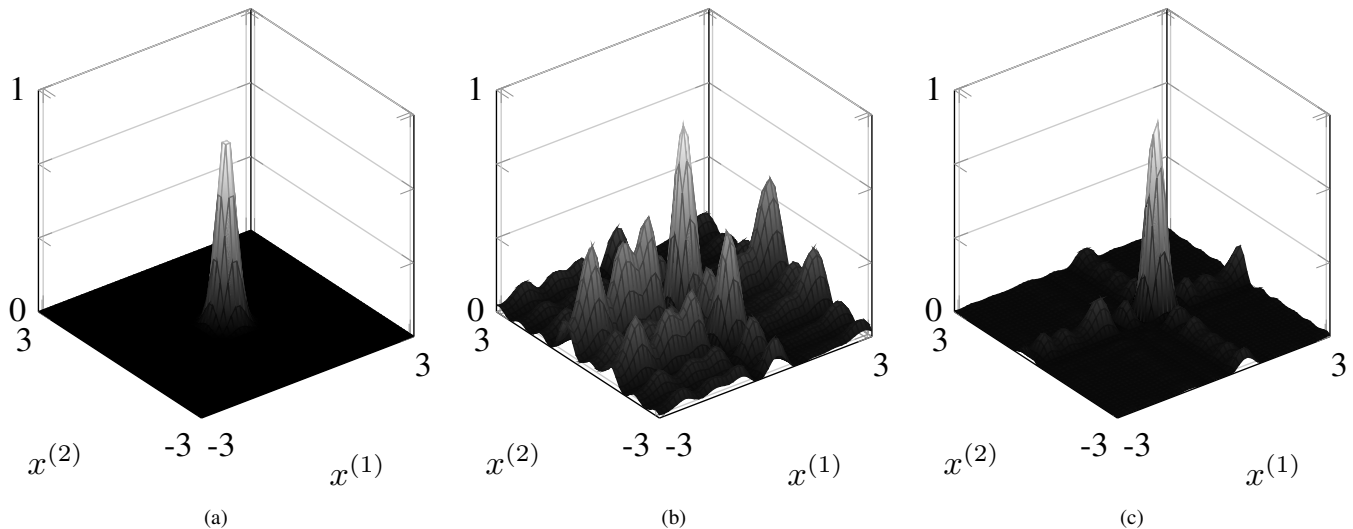


Fig. 6. Comparison between the spatial probability density function ϕ (a) and the probability density function obtained averaging over time the ergodic trajectory resulting from the implementation of the persistified environment exploration (b); (c) depicts the probability density function representing the time-averaged optimized ergodic trajectory obtained without taking into account energy constraints. $x^{(1)}$ and $x^{(2)}$ are the two components of the state vector $x \in \mathcal{E} \subset \mathbb{R}^2$.

probability density functions for the time-averaged optimized trajectory with energy constraints (Fig. 6b) and without energy constraints (Fig. 6c). Even though the latter more closely matches the spatial distribution ϕ , it does not take into account that the robot has a finite availability of energy.

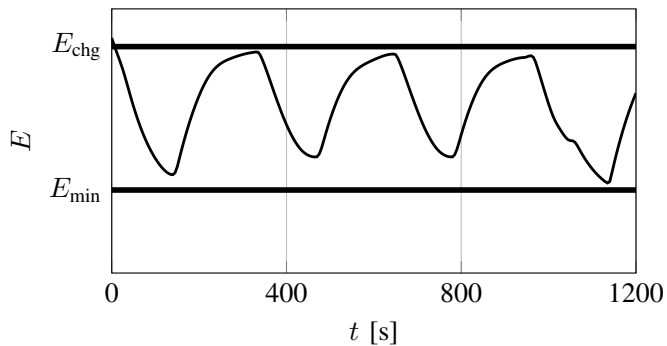


Fig. 7. Simulated battery level of the robot during the course of the persistified exploration experiment. Employing the persistification strategy presented in this paper, achieved by implementing the control input solution of the QP (24), the robot energy (thin line) is constrained within the bounds E_{\min} and E_{chg} .

In Fig. 7, the energy level of the robot during a persistified long-term exploration experiment are reported. The application of the control framework presented in this paper is demonstrated to be successful in persistifying the robotic exploration. This is realized by keeping the robot energy level constrained above a minimum value in an optimal way by means of the QP (24). This way, the robot is completely free of tracking the ergodic trajectory given as input to its motion controller, as long as its battery level is above the lower threshold E_{\min} and below the upper threshold E_{chg} , depicted as thick solid lines in Fig. 7.

B. Environment Surveillance

The second application that is considered as showcase is environment surveillance. The employment of mobile sensors improves coverage and data gathering performances compared to static sensors, whose positions are determined based on offline optimization algorithms. In this sense, mobility can allow a more efficient estimation of time-varying information fields. However, this comes at the price of higher power consumption. Most of the approaches developed so far assume that the mobile sensors are able to move for an unlimited amount of time. The control framework presented in this paper can be used to persistify such surveillance tasks.

The task of environment surveillance can be framed as a sensor coverage control problem, that is an instance of the broader optimal sensor placement problem whose applications can be found in many other disciplines, such as [37].

As in Section V-A, let the map $\phi : \mathcal{E} \mapsto \mathbb{R}_+$ represent a spatial distribution density function. It can be interpreted as a measure of the information spread over the environment \mathcal{E} or the probability that an event can take place at a location $x \in \mathcal{E}$. Moreover, let us define the locational optimization function as in [8]:

$$\mathcal{H}(\mathcal{X}, \mathcal{W}) = \sum_{i=1}^N \int_{W_i} f(\|x - x_i\|) \phi(x) dx, \quad (26)$$

where $\mathcal{X} = \{x_1, \dots, x_N\}$ are the positions of the N robots present in the environment \mathcal{E} , $\mathcal{W} = \{W_1, \dots, W_N\}$ is a partition of \mathcal{E} , $f : \mathbb{R}_+ \mapsto \mathbb{R}_+$ is a non-decreasing differentiable function describing the degradation in the sensing performances of the robots. Proceeding as in [8], we aim at minimizing $\mathcal{H}(\mathcal{X}, \mathcal{W})$ with respect to both \mathcal{X} and \mathcal{W} . The minimization with respect to the environment partition \mathcal{W} leads to $\mathcal{W} = \mathcal{V} = \{V_1, \dots, V_N\}$ [37], \mathcal{V} being the Voronoi

partition of \mathcal{E} defined by

$$V_i = \{x \in \mathcal{E} \mid \|x - x_i\| \leq \|x - x_j\| \ \forall i \neq j\}.$$

As far as the minimization with respect to the robot locations \mathcal{X} is concerned, considering the single integrator dynamics of the robots and setting $f(\|x - x_i\|) = \|x - x_i\|^2$ allow the following gradient descent update step to be used as a control law for moving the robots [38]:

$$\hat{u}_i = k_p(C_{V_i} - x_i). \quad (27)$$

In (27), $k_p > 0$ is a proportional gain and C_{V_i} is the centroid of the i -th Voronoi cell defined as:

$$C_{V_i} = \frac{\int_{V_i} x \phi(x) dx}{\int_{V_i} \phi(x) dx}.$$

In case the map ϕ is time-varying, the extension presented in [9] can be employed to synthesize a similar control law.

The coverage task with $\hat{u} = [\hat{u}_1^T, \dots, \hat{u}_N^T]^T$ and \hat{u}_i given by (27), can be persistified by the implementation of the optimization-based controller defined in (24).

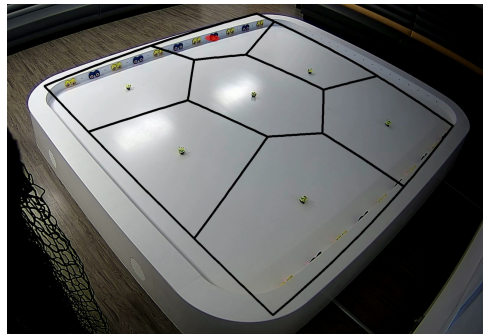
The persistified environment surveillance has been implemented and deployed onto the Robotarium, a remotely accessible swarm robotics research testbed [39]. A team of 7 differential-drive robots attempts to cover the 4.5×3.5 m testbed area by making use of the coverage control introduced above. The Robotarium is endowed with wireless charging stations, allowing the modeling of the charging field I given in (2) by means of bump-like functions as depicted in Fig. 3. The robot model is the single integrator model, where we can directly control the robots' velocities utilizing the proportional control law given in (27). This input is wrapped by the QP (24) in order to simultaneously satisfy the coverage objective and the energy constraints. This results in a persistified environment surveillance.

Figures 8a to 8d show the salient frames of the persistent environment surveillance experiment performed on the Robotarium. The Voronoi cells are superimposed on the frames. The wireless charging station (yellow and blue) are arranged along one of the edges of the testbed. Following the nominal controller (27), the robots perform sensor coverage (8a). The actual controller executed by the robots is the solution of (24), which allows them to go back and recharge their batteries to prevent the stored energy from going below the minimum desired value E_{\min} (8b, 8c and 8d).

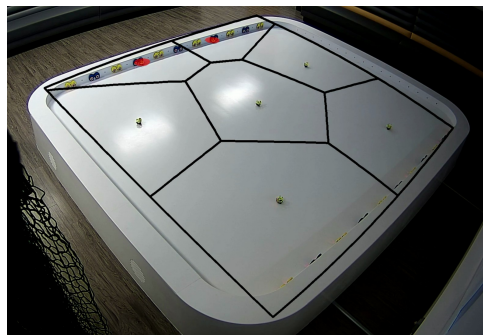
In Fig. 9 the thin line shows the value of the locational cost defined in (26) evaluated during the course of the experiment. Here the information distribution density function ϕ has been set to a constant value, meaning that the information is equally spread over the testbed. The thick line of Fig. 9 represents the value of the cost (26) obtained as if no energy constraints were imposed, in which case, the robots are able to asymptotically reach the centroidal Voronoi configuration, where each robot is in the center of its corresponding Voronoi cell. This configuration leads to a local minimum of (26). The value of \mathcal{H} decreases in correspondence of the situations in which all the available robots are not constrained to charge and are consequently free of following the coverage control input.



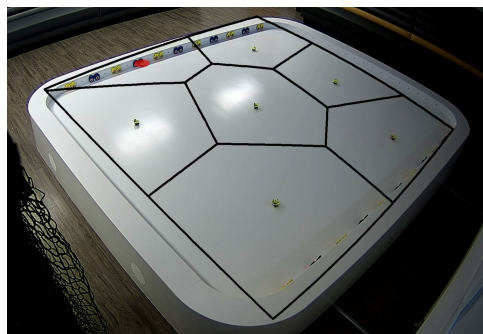
(a)



(b)



(c)



(d)

Fig. 8. Sequence of salient frames extracted from the video of the persistent environment surveillance experiment. A team of 7 small differential-drive robots are deployed to perform persistent sensor coverage of the testbed of the Robotarium. On one edge of the testbed there are wireless charging stations (yellow and blue) where the robots can recharge their batteries. The charging field has been modeled similarly to the example shown in Fig. 3. The black lines represent the boundaries of the Voronoi cells corresponding to each robot. The sequence of images shows the robots performing coverage under the nominal control input (8a), two robots, marked with red circles, going back to the charging stations to recharge their batteries (8b and 8c) driven by the controller (24).

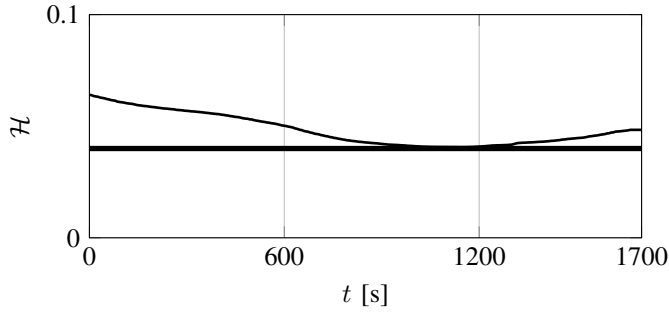


Fig. 9. Locational cost (26) evaluated during the course of a coverage control experiment: the thin line is the cost obtained imposing the energy constraints to the robots, whereas the thick line is the cost obtained assuming infinite availability of energy.

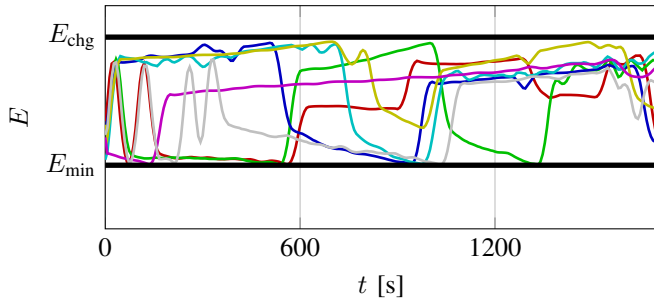


Fig. 10. Battery levels of 7 robots measured during the persistified coverage control experiment: as a result of the QP (24), the energy levels of all the robots are constrained to be between the values E_{\min} and E_{chg} .

Fig. 10 displays the energy stored in the batteries of the robots as measured during the course of the experiment. The inputs to the robots are constrained by (21) and (23), whose full expressions are given in Appendix A, in such a way that their energies never exceeds E_{chg} , while never going below E_{\min} either. As a results of the formulation as an optimization problem (24), each individual robot is able to follow as closely as possible the input encoding the coverage task as long as its battery level satisfies the imposed constraints.

VI. CONCLUSIONS

In this paper we introduced the concept of robotic task persistification, i. e., the process of rendering a robotic task persistent. This allows robots to execute a task over long time horizons, by ensuring that the energy stored in their batteries never gets depleted. The control of the robot energy level is wrapped around the task controller by utilizing control barrier functions (CBFs) and control Lyapunov functions (CLFs) combined in a single optimization-based controller which can be efficiently executed in online settings. The result of this formulation is a control framework that allows the robots to execute as closely as possible the assigned task, while simultaneously never depleting the energy in their batteries. This constraint is enforced by expressing the persistency condition in terms of the forward invariance of a subset of the state space of the robots. The forward invariance property is then enforced with the aid of control barrier functions. The

battery recharging is instead achieved by defining a suitable control Lyapunov function.

Theorems 9, Lemma 12 and 16 allow us to apply the presented framework to many different kinds of robots endowed with rechargeable, or even interchangeable, sources of energy. In order to be able to efficiently enforce energy constraints, we insist on the robot dynamic model being in control affine form, case that is often encountered in robotic applications. Since the persistified task is obtained as the output of an optimization problem, the robots are free to execute the given task as closely as possible as long as their source of energy is not discharging below a given lower threshold. The persistification strategy has been applied to environment exploration and monitoring tasks, and it has been tested both in simulation and on an team of ground mobile robots on the Robotarium.

APPENDIX A

For single integrator robot dynamics and the CBFs (19) and (20), the expressions of $\frac{\partial h_{i2}}{\partial t}$, $L_f^2 h_{i1}$ and $L_g L_f h_{i1}$ required to evaluate (21) are given by:

$$\begin{aligned} \frac{\partial h_{i2}}{\partial t} &= (E_{\text{chg}} + E_{\min} - 2E_i) \frac{\partial F}{\partial w} \frac{\partial w}{\partial I} \frac{\partial I}{\partial t} = \\ &= (E_{\text{chg}} + E_{\min} - 2E_i) k w^2 \frac{1 - E_i}{E_i} \lambda e^{-\lambda(I(x_i, t) - I_c)} \frac{\partial I}{\partial t} \end{aligned}$$

$$\begin{aligned} L_f^2 h_{i1} &= \left(-2F(x_i, E_i, t) + \right. \\ &\quad \left. + (E_{\text{chg}} + E_{\min} - 2E_i) \frac{\partial F}{\partial E_i} \right) F(x_i, E_i, t) \end{aligned}$$

$$\begin{aligned} L_g L_f h_{i1} &= (E_{\text{chg}} + E_{\min} - 2E_i) \frac{\partial F}{\partial w} \frac{\partial w}{\partial I} \frac{\partial I}{\partial x_i} = \\ &= (E_{\text{chg}} + E_{\min} - 2E_i) k w^2 \frac{1 - E_i}{E_i} \lambda e^{-\lambda(I(x_i, t) - I_c)} \frac{\partial I}{\partial x_i} \end{aligned}$$

For single integrator robot dynamics and the CLF (22), the expressions of $\frac{\partial h_{i2}}{\partial t}$, $L_f^2 V_i$ and $L_g L_f V_i$ required to evaluate (23) are given by:

$$\begin{aligned} \frac{\partial h_{i2}}{\partial t} &= -2(E_{\text{chg}} - E_i) \frac{\partial F}{\partial w} \frac{\partial w}{\partial I} \frac{\partial I}{\partial t} = \\ &= -2(E_{\text{chg}} - E_i) k w^2 \frac{1 - E_i}{E_i} \lambda e^{-\lambda(I(x_i, t) - I_c)} \frac{\partial I}{\partial t}, \\ L_f^2 V_i &= \left(2F(x_i, E_i, t) - 2(E_{\text{chg}} - E_i) \frac{\partial F}{\partial E_i} \right) F(x_i, E_i, t), \\ L_g L_f V_i &= -2(E_{\text{chg}} - E_{\min}) \frac{\partial F}{\partial w} \frac{\partial w}{\partial I} \frac{\partial I}{\partial x_i} = \\ &= -2(E_{\text{chg}} - E_{\min}) k w^2 \frac{1 - E_i}{E_i} \lambda e^{-\lambda(I(x_i, t) - I_c)} \frac{\partial I}{\partial x_i}. \end{aligned}$$

REFERENCES

- [1] A. Ollero, S. Lacroix, L. Merino, J. Gancet, J. Wiklund, V. Remuß, I. V. Perez, L. G. Gutiérrez, D. X. Viegas, M. A. G. Benitez *et al.*, "Multiple eyes in the skies: architecture and perception issues in the comets unmanned air vehicles project," *IEEE robotics & automation magazine*, vol. 12, no. 2, pp. 46–57, 2005.
- [2] E. Fiorelli, N. E. Leonard, P. Bhatta, D. A. Paley, R. Bachmayer, and D. M. Fratantoni, "Multi-aUV control and adaptive sampling in monterey bay," *IEEE journal of oceanic engineering*, vol. 31, no. 4, pp. 935–948, 2006.

- [3] N. E. Leonard, D. A. Paley, R. E. Davis, D. M. Fratantoni, F. Lekien, and F. Zhang, "Coordinated control of an underwater glider fleet in an adaptive ocean sampling field experiment in monterey bay," *Journal of Field Robotics*, vol. 27, no. 6, pp. 718–740, 2010.
- [4] R. Graham and J. Cortés, "Adaptive information collection by robotic sensor networks for spatial estimation," *IEEE Transactions on Automatic Control*, vol. 57, no. 6, pp. 1404–1419, 2012.
- [5] B. Kuipers and Y.-T. Byun, "A robot exploration and mapping strategy based on a semantic hierarchy of spatial representations," *Robotics and autonomous systems*, vol. 8, no. 1, pp. 47–63, 1991.
- [6] R. O'Flaherty and M. Egerstedt, "Optimal exploration in unknown environments," in *Intelligent Robots and Systems (IROS), 2015 IEEE/RSJ International Conference on*. IEEE, 2015, pp. 5796–5801.
- [7] W. Burgard, M. Moors, D. Fox, R. Simmons, and S. Thrun, "Collaborative multi-robot exploration," in *Robotics and Automation, 2000. Proceedings. ICRA'00. IEEE International Conference on*, vol. 1. IEEE, 2000, pp. 476–481.
- [8] J. Cortes, S. Martinez, T. Karatas, and F. Bullo, "Coverage control for mobile sensing networks," *IEEE Transactions on robotics and Automation*, vol. 20, no. 2, pp. 243–255, 2004.
- [9] S. G. Lee, Y. Diaz-Mercado, and M. Egerstedt, "Multirobot control using time-varying density functions," *IEEE Transactions on Robotics*, vol. 31, no. 2, pp. 489–493, 2015.
- [10] A. Krause, A. Singh, and C. Guestrin, "Near-optimal sensor placements in gaussian processes: Theory, efficient algorithms and empirical studies," *Journal of Machine Learning Research*, vol. 9, no. Feb, pp. 235–284, 2008.
- [11] M. Morris and S. Tosunoglu, "Survey of rechargeable batteries for robotic applications."
- [12] D. Mitchell, M. Corah, N. Chakraborty, K. Sycara, and N. Michael, "Multi-robot long-term persistent coverage with fuel constrained robots," in *Robotics and Automation (ICRA), 2015 IEEE International Conference on*. IEEE, 2015, pp. 1093–1099.
- [13] B. Bethke, J. How, and J. Vian, "Multi-uav persistent surveillance with communication constraints and health management," in *AIAA Guidance, Navigation, and Control Conference*, 2009, p. 5654.
- [14] J. Derenick, N. Michael, and V. Kumar, "Energy-aware coverage control with docking for robot teams," in *Intelligent Robots and Systems (IROS), 2011 IEEE/RSJ International Conference on*. IEEE, 2011, pp. 3667–3672.
- [15] N. Kamra and N. Ayanian, "A mixed integer programming model for timed deliveries in multirobot systems," in *Automation Science and Engineering (CASE), 2015 IEEE International Conference on*. IEEE, 2015, pp. 612–617.
- [16] N. Mathew, S. L. Smith, and S. L. Waslander, "Multirobot rendezvous planning for recharging in persistent tasks," *IEEE Transactions on Robotics*, vol. 31, no. 1, pp. 128–142, 2015.
- [17] L. Liu and N. Michael, "Energy-aware aerial vehicle deployment via bipartite graph matching," in *Unmanned Aircraft Systems (ICUAS), 2014 International Conference on*. IEEE, 2014, pp. 189–194.
- [18] A. D. Ames, J. W. Grizzle, and P. Tabuada, "Control barrier function based quadratic programs with application to adaptive cruise control," in *Decision and Control (CDC), 2014 IEEE 53rd Annual Conference on*. IEEE, 2014, pp. 6271–6278.
- [19] A. D. Ames, X. Xu, J. W. Grizzle, and P. Tabuada, "Control barrier function based quadratic programs for safety critical systems," *IEEE Transactions on Automatic Control*, 2016.
- [20] Q. Nguyen and K. Sreenath, "Exponential control barrier functions for enforcing high relative-degree safety-critical constraints," in *American Control Conference (ACC), 2016*. IEEE, 2016, pp. 322–328.
- [21] G. Wu and K. Sreenath, "Safety-critical control of a planar quadrotor," in *American Control Conference (ACC), 2016*. IEEE, 2016, pp. 2252–2258.
- [22] G. Notomista, S. Ruf, and M. Egerstedt, "Persistification of robotic tasks using control barrier functions," *IEEE Robotics and Automation Letters*, 2018.
- [23] S. M. LaValle, *Planning algorithms*. Cambridge university press, 2006.
- [24] C. Daniel and J. O. Besenhard, *Handbook of battery materials*. John Wiley & Sons, 2012.
- [25] G. Notomista, Y. Emam, and M. Egerstedt, "The slothbot: A novel design for a wire-traversing robot," *IEEE Robotics and Automation Letters*, 2019 (in press).
- [26] L. W. Tu, "Bump functions and partitions of unity," *An Introduction to Manifolds*, pp. 127–134, 2008.
- [27] X. Xu, P. Tabuada, J. W. Grizzle, and A. D. Ames, "Robustness of control barrier functions for safety critical control** this work is partially supported by the national science foundation grants 1239055, 1239037 and 1239085." *IFAC-PapersOnLine*, vol. 48, no. 27, pp. 54–61, 2015.
- [28] C. M. Kellett, "A compendium of comparison function results," *Mathematics of Control, Signals, and Systems*, vol. 26, no. 3, pp. 339–374, 2014.
- [29] H. K. Khalil, "Nonlinear systems, 3rd," *New Jersey, Prentice Hall*, vol. 9, 2002.
- [30] J. Garche and A. Jossen, "Battery management systems (bms) for increasing battery life time," in *Telecommunications Energy Special Conference, 2000. TELESCON 2000. The Third International*. IEEE, 2000, pp. 81–88.
- [31] S. Boyd and L. Vandenberghe, *Convex optimization*. Cambridge university press, 2004.
- [32] Y. Girdhar and G. Dudek, "Modeling curiosity in a mobile robot for long-term autonomous exploration and monitoring," *Autonomous Robots*, vol. 40, no. 7, pp. 1267–1278, 2016.
- [33] J. G. Bellingham and K. Rajan, "Robotics in remote and hostile environments," *Science*, vol. 318, no. 5853, pp. 1098–1102, 2007.
- [34] M. Dunbabin and L. Marques, "Robots for environmental monitoring: Significant advancements and applications," *IEEE Robotics & Automation Magazine*, vol. 19, no. 1, pp. 24–39, 2012.
- [35] L. M. Miller and T. D. Murphey, "Trajectory optimization for continuous ergodic exploration," in *American Control Conference (ACC), 2013*. IEEE, 2013, pp. 4196–4201.
- [36] G. Mathew and I. Mezić, "Metrics for ergodicity and design of ergodic dynamics for multi-agent systems," *Physica D: Nonlinear Phenomena*, vol. 240, no. 4, pp. 432–442, 2011.
- [37] A. Okabe and A. Suzuki, "Locational optimization problems solved through voronoi diagrams," *European Journal of Operational Research*, vol. 98, no. 3, pp. 445–456, 1997.
- [38] M. Mesbahi and M. Egerstedt, *Graph theoretic methods in multiagent networks*. Princeton University Press, 2010.
- [39] D. Pickem, P. Glotfelter, L. Wang, M. Mote, A. Ames, E. Feron, and M. Egerstedt, "The robotarium: A remotely accessible swarm robotics research testbed," in *Robotics and Automation (ICRA), 2017 IEEE International Conference on*. IEEE, 2017, pp. 1699–1706.